31st Annual International Conference of the IEEE EMBS
Minneapolis, Minnesota, USA, September 2-6, 2009

Automated Liver Segmentation for Whole-Body Low-Contrast CT Images from PET-CT Scanners

Xiuying Wang, Changyang Li, Stefan Eberl, Michael Fulham and Dagan Feng

Abstract—**Accurate objective automated liver segmentation in PET-CT studies is important to improve the identification and localization of hepatic tumor. However, this segmentation is an extremely challenging task from the low-contrast CT images captured from PET-CT scanners because of the intensity similarity between liver and adjacent loops of bowel, stomach and muscle. In this paper, we propose a novel automated three-stage liver segmentation technique for PET-CT whole body studies, where: 1) the starting liver slice is automatically localized based on the liver – lung relations; 2) the "masking" slice containing the biggest liver section is localized using the ratio of liver ROI size to the right half of abdomen ROI size; 3) the liver segmented from the "masking" slice forms the initial estimation or mask for the automated liver segmentation. Our experimental results from clinical PET-CT studies show that this method can automatically segment the liver for a range of different patients, with consistent objective selection criteria and reproducible accurate results.**

I. INTRODUCTION

MEDICAL imaging has an integral role in the diagnosis and management of liver diseases, in particular in the detection / localization and characterization of various types of malignancy [1]. On occasions it can be problematic to characterize lesions that lie adjacent to but not involve the liver such as thoracic tumors involving the lateral costophrenic angles overlying the liver surface and tumors in bowel or adjacent stomach that abut the liver surface. Liver segmentation from multimodal and monomodal medical images thus can have an important role in clinical management [2]. However, the anatomical relationships to adjacent organs – the diaphragm, costophrenic angles, lower chest wall, right kidney, stomach and bowel – mean that automated liver segmentation from CT images is a challenging task. Many of these organs have similar densities on non-contrast enhanced CT scans and so it is difficult to extract the liver boundaries by conventional segmentation techniques based on grey level intensities [3]. The hepatic parenchyma can also have a different appearance between patients due to fatty infiltration and the scan technique [4].

Segmentation methods based on grey levels are widely used for automated liver segmentation from CT images. Based on these methodologies, statistical analysis [4, 5, 6] and clinical knowledge analysis [7] have been proposed to improve the accuracy and performance of liver segmentation. Registration-enhanced deformable segmentation was applied on the liver segmentation [8]. However, these methods might fail to accurately segment the liver because of large inter-patient and intra-patient grey level variability.

Combined PET-CT scans provide anatomical (CT) and functional (PET) information. Through the identification of regions of increased FDG uptake (or "hotspots") on PET, which are typically found with liver tumors and where the CT can be normal, PET-CT is often now used as a staging investigation [9] and also to assess response to therapy. Unlike conventional, multi-phase, contrast-enhanced hepatic CT imaging PET-CT scanners provide low-contrast CT images. Thus any automated liver segmentation from these low-contrast CT images is consequently more challenging. Further, current semi-automatic or automatic liver segmentation approaches for the high-contrast CT images are not directly applicable to low-contrast CT. In this paper, we propose a method, which aims to accurately identify the gray level intensities of the liver on the basis of clinical knowledge, and automatically segments the liver from the low-contrast CT images that are captured from the combined PET-CT.

II. PROPOSED METHOD

The framework of our algorithm is shown in Fig.1. The preprocessing step includes removal of background noise and the patient bed; then using the topological relationship between the lung and liver, the starting liver slice is determined. The "masking" slice, which contains the biggest liver section, is then localized automatically based on the ratio of liver region of interest (ROI) size to the right half of abdomen (LTRA) ROI size. The automated segmentation is then performed sequentially over the whole liver volume that

Manuscript received April 23, 2009. This work was supported by ARC and PolyU grants.

X. Wang C. Li are with the Biomedical and Multimedia Information Technology (BMIT) Research Group, School of Information Technologies, University of Sydney, Australia (e-mails: xiuying@it.usyd.edu.au; chli7560@it.usyd.edu.au).

S. Eberl is with the BMIT Research Group, School of Information Technologies, University of Sydney, Australia, and Department of PET and Nuclear Medicine, Royal Prince Alfred Hospital (RPAH), Sydney, Australia (e-mail: stefan@cs.usyd.edu.au).

M. Fulham is with the BMIT Research Group, School of Information Technologies, and Faculty of Medicine, University of Sydney, Australia, and Department of PET and Nuclear Medicine, Royal Prince Alfred Hospital (RPAH), Sydney, Australia (e-mail: mfulham@med.usyd.edu.au).

D. Feng is with the BMIT Research Group, School of Information Technologies, University of Sydney, Australia, and Center for Multimedia Signal Processing (CMSP), Dept. of Electronic & Information Engineering, Hong Kong Polytechnic University, and Med-X Research Institute, Shanghai JiaoTong University, China (e-mail: feng@it.usyd.edu.au).

is based on the "masking slice" obtained.

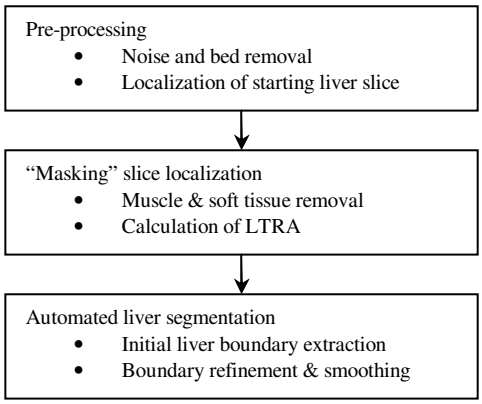

Fig.1. Framework of automated liver segmentation.

A. Stage one: Pre-processing

1) Noise and patient bed removal: The background and patient bed are removed from the raw clinical data as an initial step to improve the accuracy of the segmentation. The Hounsfield unit (HU) of the background noise is much lower than other information in the image and so with histogram analysis the noise is successfully removed by a single threshold (-400HU in our experiments). Based on our previous work on automated lung segmentation [10], the pre-processing of the bed removal starts with the first lung slice. Then, applying the flood-fill operation to both the abdomen and bed regions, the biggest connected region that represents the abdominal region can be determined and the remaining bed region is removed.

2) Automated localization of starting liver slice: Based on our automated lung segmentation [10] and by utilizing the topological relationship of lung and liver, our algorithm firstly detects the starting liver slice from the whole body volume.

The intensity values of the lungs are very different from the liver values. The right lung axial slices are detected from the bottom-up to identify the first liver slice. In this sequence of bottom-up lung slices, the size of the liver ROI residing inside the right lung decreases slice by slice. The slice where the size of the liver ROI reduces to < 150 pixels is considered as the starting liver slice in our algorithm.

B. Stage two: "Masking" liver slice localization

1) Ratio of liver ROI size to the right half of the abdomen (LTRA) ROI size: Our algorithm is based on the "masking" slice proposed by Bae, et al [5] and extended to liver segmentation with the gradient vector flow (GVF) method [11] to initialize the segmentation. The "masking" slice containing the biggest liver region can prevent the deformable model leaking into other organs and improve the efficiency of the algorithm [11]. However, the localization of the "masking" slice in these methods is not fully automated and requires user interaction.

In our algorithm, the knowledge that the liver occupies the majority of right half of corresponding abdominal section, is utilized to localize the "masking" slice automatically. Based on this prior knowledge, LTRA (as Equ. 1), is used to localize the "masking" image.

$$\mathrm{LTRA}(x) = \frac{\mathrm{LROI}(x)}{\mathrm{RA}(x)} \qquad (1)$$

where LROI(x) is the number of liver ROI pixels, and RA(x) is the number of pixels of the right half of the abdominal region. The centroid of the vertebral column is used to separate the right and left halves of the abdomen. The pixels with value greater than 0HU in the region of right half of the abdomen are classified as the liver ROI [12].

However, because soft tissue and muscle vary across the patients, the LTRA spans a wide range of values. Bae, et al [5] identified that even for the same liver volume, the ratio distribution ranged from 10% to 32.2% for different slices with relative big liver regions. Therefore, the biggest LTRA does not reliably identify the "masking" liver slice. To localize an accurate "masking" slice automatically, muscle must be removed before the calculation of LTRA.

Differentiating muscle from liver can be difficult even for high-contrast CT images. Lim, et.al [4] and Gao, et al [13] used morphological filters to remove the muscle adjacent to the liver. In low-contrast CT images, the intensity distribution of muscle lying adjacent to the liver region overlaps that of the liver and therefore the histogram analysis is not helpful.

2) Muscle removal: The muscles of the lower chest wall and upper abdomen overlying the liver are interspersed with ribs in the right upper quadrant of the abdomen. Ribs have high density values and are readily extracted. The extracted ribs provide sufficient inflation force to prevent the balloon active contour overflowing into the muscle, and can guide the balloon active contour to exclude the muscle around the liver region. This muscle removal procedure peels both muscle and soft tissue (fat and skin) outside the ribs. This strategy is applied to the right side of the abdomen to hasten the muscle removal. With this approach, after muscle removal, the LTRAs of the 'masking' slices for different patients' datasets can be fitted in the range of 75% to 82%.

C. Stage three: Automated liver segmentation

1) Initial liver ROI segmentation by histogram analysis: After muscle and soft tissue removal, the histogram of the first "masking" slice with the highest LTRA has a single major peak, which includes majority of pixels being corresponded to the liver ROI, and is used to extract the initial liver ROI by adaptive thresholding. The method can overcome streak artifacts produced by the "arms-down" position into liver region [14].

2) Refinement and smoothing: After the thresholding, most of neighboring organs and tissues are removed. Parts of internal organs and neighboring tissues, however, still

remain. Morphological operations are then performed to remove these objects and preserve the complete liver region. An opening operation, with a 3-by-3 disc-structuring element, is used to disconnect and remove neighboring structures connected to the liver object.

This stage of refinement and smoothing is required to reach the real liver boundary. We employed the level-set algorithm to refine the liver boundary and used the image-based features in the governing differential equation [15]. Two input images are required by this algorithm: the binary image after the morphological operations as the best guess position, and the original image as the feature image.

3) The segmentation of whole liver volume: The segmented liver region from the "masking" slice is the biggest liver section in the axial view, and therefore, it can be used as a mask for the liver ROI in the other slices of the liver volume. However, the position, the size and the shape of the liver ROI may vary across the slices. To provide full coverage of the liver ROI, the mask slice is anisotropically dilated by using the disk illustrated in the figure 2. To avoid error accumulation, the mask is replaced by the current segmented liver region every three slices.

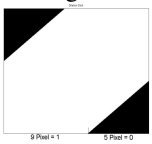

Fig.2. Dilation disk.

III. Experimental Results and Discussion

A. Clinical datasets

We validated our method on clinical PET-CT studies from the Royal Prince Alfred (RPA) Hospital. CT acquisition settings were 120kVp. The CT images were 512 * 512 pixels with 16-bit quantization and 3mm thickness.

B. Automated liver segmentation procedure

Fig.3 illustrates the step-by-step automated liver segmentation procedure from whole-body CT volumes.

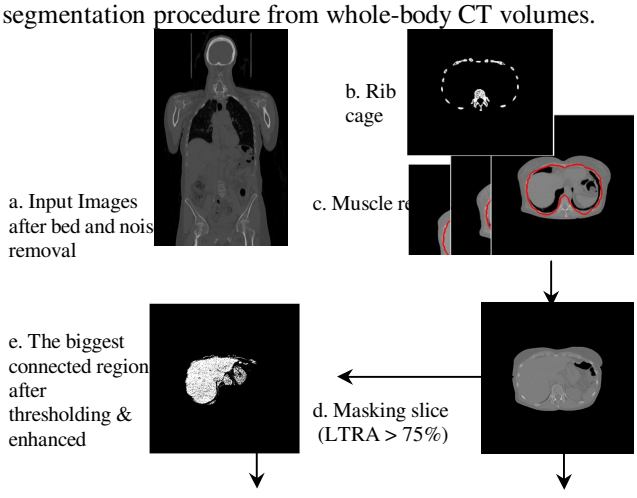

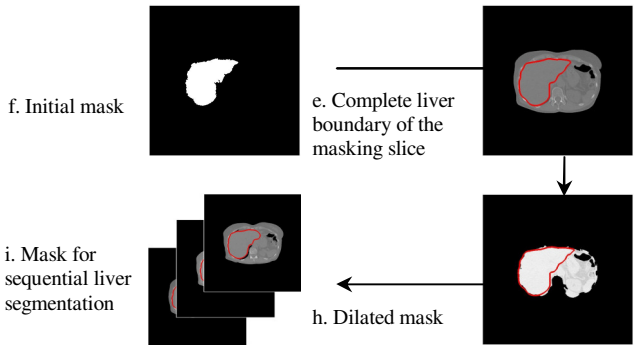

Fig .3. Step by step segmentation procedure.

C. Effect of removing muscle

The three histograms in Fig.4 represent segmented soft tissues and muscle regions and liver regions for the "masking" slice from three different CT volumes. The much lower fat density value means it is easily removed with a single threshold. The statistical data show that the muscle overlaps with the liver density range (~0 HU to 100 HU). The extracted ribs when used as the guidance for balloon active contouring, solves this problem.

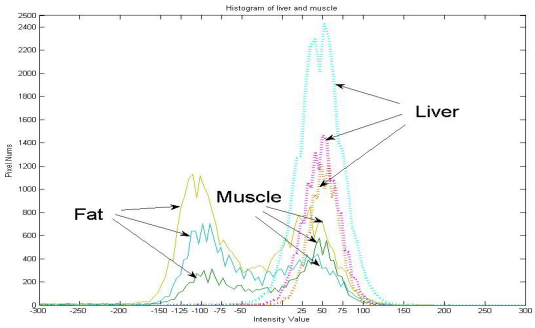

Fig. 4. The histograms of segmented fat & muscle and liver from three clinical CT datasets to demonstrate that muscle and liver overlap over the same intensity range (~ 0HU to 100HU).

The histograms in the Fig.5 illustrate the effect of muscle removal in the "masking" slice. The histogram of the image after muscle and fat removal contains predominately pixels belonging to the liver region. The step of muscle removal is important to improve the accurate masking slice extraction and liver segmentation from low-contrast CT images.

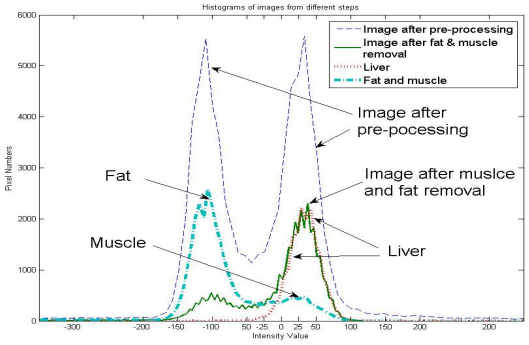

Fig.5. The histograms of the image after pre-processing, the segmented fat and muscle, the segmented liver, and after removal of fat and muscle.

D. Experimental results of the automated liver segmentation

We tested the algorithm on clinical low-contrast CT images from 10 different patients of varying sizes and shapes for validation. Because positioning patient with "arms down" or "arms-up" affects the CT image quality [14], we evaluated our algorithm on datasets with the "arms-down" (Fig. 6.a and b) and the "arms-up" (Fig. 6.c and d). Although the "arms-down" position may introduce streak artifacts into the liver region in CT images, our results show, based on visual assessment that our algorithm can accurately and automatically segment the liver from the neighboring organs such as heart and stomach.

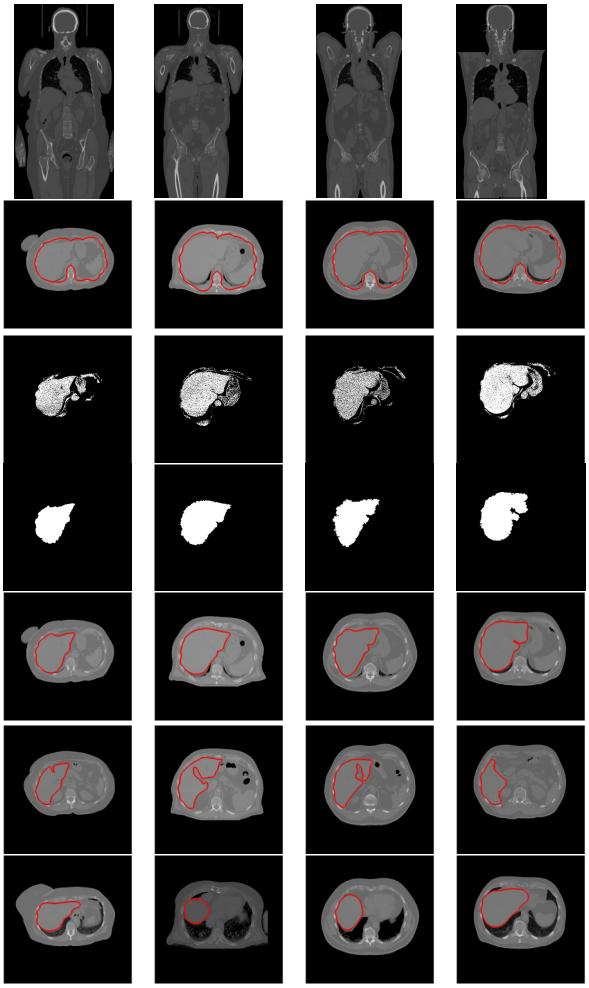

Fig. 6. Experimental results in patients with arms down (column a and b) and arms up (column c and d): 1st row: input images after noise and bed removal; 2nd row: muscle removal and "masking" slice identified; 3rd row: the biggest connected region after thresholding; 4th row: initial mask; 5th row: complete liver boundary of the "masking "slice; 6th row: sequential liver segmentation below the "masking "slice (5th row); 7th row: sequential liver segmentation above the "masking" slice (5th row).

IV. Conclusion

We propose a fully automated liver segmentation method for whole-body low-contrast CT images. The method can improve the delineation of low-contrast anatomy between the liver and the adjacent and surrounding tissues and organs that have similar intensities. Our experimental results with clinical data indicate that our automated algorithm can correctly segment the liver in a variety of patients.

References

[1] Oliva, M. R. & Saini, S. 2004. Liver cancer imaging: role of CT, MRI, US and PET. *Cancer Imaging*, 4(spec no A):S42–S46.

[2] Sojar, V., Stanisavljev, D., Hribernik, M., Glui, M., Kreuh, D., Velkavrh, U. & Fius, T. 2004. Liver surgery training and planning in 3D virtual space. *Proceedings of the 18th International Congress and Exhibition, Compuer Assited Radiology and Surgery*, 1268, 390–394.

[3] Campadelli, P. & Casiraghi, E. 2007. Liver Segmentation from CT Scans: A Survey. *Lecture Notes in Computer Science*, Volume 4578/2007, 520-528, Berlin/Heidelberg: Springer.

[4] Lim, S. J., Jeong, Y.Y. & Ho, Y. S. 2006. Automatic liver segmentation for volume measurement in CT images. *Journal of Visual Communication and Image Representation*, 17(4), 860-875.

[5] Bae, K. T., Giger, M. L., Chen, C. T., Kahn, C. E. 1993. Automatic segmentation of liver structure in CT images. *Medical Physics,* 20(1), 71-78.

[6] Lim, S. J., Jeong, Y.Y. & Ho, Y. S. 2005. Segmentation of the liver using the deformable contour method on CT images. In: *Proceedings of SPIE*, vol. 3767, pp. 570–581.

[7] Camara, O., Colliot, O. and Bloch, I. 2004. Computational modeling of thoracic and abdominal anatomy using spatial relationships for image segmentation. *Imaging in Bioinformatics*, volume 10 Issue 4, pp. 263-273.

[8] Soler, L., Delingette, H., Malandain, G., Montagnat, J., Ayache, N., Koehl, C., Dourthe, O., Malassagne, B., Smith, M., Mutter, D., Marescaux, J. 2001. Fully automatic anatomical, pathological, and functional segmentation from ct scans for hepatic surgery. *Computed Aided Surgery* 6 (3), pp.131–142.

[9] Cohade, C., Osman, M., Leal, J. & Wahl, R.L.2003. Direct Comparison of 18F-FDG PET and PET/CT in Patients with Colorectal Carcinoma. *The Journal of Nuclear Medicine*, 44(11), 1797-1803.

[10] Ballangan, C., Wang, X. Y., Feng, D.G., Stefan, E., Michael, F. 2008. Lung segmentation and tumor detection from CT thorax volumes of FDG PET-CT scans by template registration and incorporation of functional information. *IEEE Nuclear Science Symposium Conference Record*, 5349-5353.

[11] Liu, F., Zhao, B. S., Kijewski, P. K., Wang, L. & Schwartz, L. H. 2005. Liver segmentation for CT images using GVF snake. *Medical Physics*, 32(12), 3699–3706.

[12] Lee, F. T., Chosy, S. G., Naidu, S. G., Goldfarb, S., Weichert, J. P., Bakan, D. A., Kuhlman, J. E., Tambeaux, R. H. & Sproat, I. A. 1997. CT depiction of experimental liver tumors: contrast enhancement with hepatocyte-selective iodinated triglyceride versus conventional techniques. *Radiology*, 203(2), 465-470.

[13] Gao, L., Heath, D. G., Kuszyk, B. S. & Fishman, E. K.1996. Automatic liver segmentation technique for three-dimensional visualization of CT data. *Radiology*, 201, 359–364.

[14] Beyer, T., Antoch, G., Mu¨ller, S., Egelhof, T., Freudenberg, L. S., Debatin, J. & Bockisch, A. 2003. Acquisition protocol considerations for combined PET/CT imaging. *The Journal of Nuclear Medicine,* 45(1), 25S-35S.

[15] Chen, Y.F., Zhao, W. D., Wang, Z. C. 2007. Level Set Segmentation Algorithm Based on Image Entropy and Simulated Annealing. *Bioinformatics and Biomedical Engineering*, 999 – 1003.